



Positron annihilation study of the vacancy clusters in ODS Fe-14Cr alloys

Journal:	<i>Philosophical Magazine & Philosophical Magazine Letters</i>
Manuscript ID	TPHM-16-Jan-0037
Journal Selection:	Philosophical Magazine
Date Submitted by the Author:	22-Jan-2016
Complete List of Authors:	Domínguez-Reyes, Ricardo; Universidad Carlos III de Madrid, Physics Auger, María; University of Oxford, Department of Materials; Universidad Carlos III de Madrid, Physics Monge, Miguel; Universidad Carlos III de Madrid, Physics Pareja, Ramiro; Universidad Carlos III de Madrid, Physics
Keywords:	positron annihilation, steel, alloys
Keywords (user supplied):	ODS alloys, vacancy clusters

SCHOLARONE™
Manuscripts

Positron annihilation study of the vacancy clusters in ODS Fe-14Cr alloys

R. Domínguez-Reyes^{a*}, M. A. Auger^{a,b}, M. A. Monge^a and R. Pareja^a

^aDepartamento de Física, Universidad Carlos III de Madrid, Avda. de la Universidad 30. 28911 Leganés, Madrid, Spain.

^bDepartment of Materials, University of Oxford. OX1 3PH Oxford, UK.

* Corresponding author. E-mail address: rdomingu@fis.uc3m.es (R. Domínguez-Reyes)

Positron annihilation study of the vacancy clusters in ODS Fe-14Cr alloys

Oxide dispersion strengthened Fe14Cr and Fe14CrWTi alloys produced by mechanical alloying and hot isostatic pressing were subjected to isochronal annealing up to 1400 °C, and the evolution and thermal stability of the vacancy type defects were investigated by positron annihilation spectroscopy. The results were compared to those from a non-oxide dispersion strengthened Fe14Cr alloy produced by following the same powder metallurgy route. The long lifetime component of the positron annihilation spectra revealed the existence of tridimensional vacancy clusters, or nanovoids, in all these alloys. Two recovery stages are found in the oxide dispersion strengthened alloys irrespective of the starting conditions of the samples. The first one starting at $T > 750$ °C is attributed to thermal shrinkage of large vacancy clusters, or voids. A strong increase in the intensity of the long lifetime after annealing at temperatures in the 800 - 1050 °C range indicates the development of new vacancy clusters. These defects appear to be unstable above 1050 °C, but some of them remain at temperatures as high as 1400 °C, at least for 90 min.

Keywords: word; positron annihilation, steel, ODS alloys, vacancy clusters

1. Introduction

Dispersion strengthened ferritic Fe-Cr alloys with Y_2O_3 addition are presently considered one of the most promising structural materials for the future fusion reactors and generation IV fission reactors due to their enhanced high temperature strength, microstructural stability, radiation resistance, and good creep resistance at high temperature [1-4]. The appropriate powder metallurgy processing of these alloys develops a homogeneous dispersion of nano-sized hard particles that governs these mandatory properties. Analytical transmission electron microscopy (TEM) and atom probe tomography (APT) studies have contributed to reveal the dimensional, structural and compositional characteristics of the nanoparticles present in these alloys [5-9]. The

fundamental elements of these nano-features are O, Y and Cr, and some alloying impurities intentionally or accidentally added such as Ti, Al or Si [10-13], which appear to refine the size and increase the number density and stability of these nano-features. Experimental evidences for defective nanoclusters, or nano-features, in the ODS steel with a nominal composition Fe-14Cr-3.0W-0.4Ti-0.24Y₂O₃ (wt%), denoted as 14YWTi, have been found from analytical and high resolution transmission electron microscopy (TEM) studies [8]. There are also positron annihilation spectroscopy (PAS) results that point out certain association between vacancy clusters, or nanovoids, and the oxide dispersion in ODS steels [14-16]. It should be noticed that there are PAS results showing vacancy clustering, as well the opposite, in non-ODS steels processed following a powder metallurgy (PM) route similar to the ODS ones, i.e. mechanical alloying (MA) and hot isostatic pressing (HIP) consolidation [14, 17]. It is the case of the non-ODS steels with nominal composition Fe-12wt%Cr showing no evidence of tridimensional vacancy clusters in the as-HIP condition, but these clusters were detected after a heat treatment at 850 °C [17]. These results suggest that the designedly addition of solutes such as Y and Ti would not be the decisive factors for vacancy clustering associated to the oxide nano-features in the ODS steels but the processing conditions and the thermal history of the alloy.

To evidence the above and provide a better understanding on the role of the vacancies in the formation of nano-features in the ODS steels, and on the vacancy cluster behavior, a series of comprehensive isochronal annealing experiments and PAS measurements have been accomplished in ODS Fe14Cr alloys, with and without (W+Ti) addition, and in the counterpart non-ODS Fe14Cr alloy. PAS is a successful technique to study vacancy-type defects in metals and alloys [18]. Lattice defects such as vacancies, voids, solute-vacancy complexes and other open-volume defects are

effective traps for thermalized positrons in a solid. When a positron annihilates trapped in a defect, the annihilation radiation conveys information about the defect. The positron lifetime distribution provides information on the type, size and concentration of the defects. In addition, the Doppler broadening of the annihilation radiation peak at 511 keV, which depends on the momentum of the electrons annihilating with the thermalized positrons, can give information about the chemical surround of the positron annihilation sites [19, 20]. Thus, the concurrent positron lifetime spectroscopy (PLS) and coincidence Doppler broadening (CDB) measurements in isochronally annealed samples would contribute to assess the recovery kinetics of the vacancy defects and their stability in relation with the solute impurities in the ODS alloys. The understanding and assessment of these subjects are of prime interest for developing irradiation-resistant and high-temperature alloys for structural applications. The stability and recovery of radiation-induced defects would be associated with the inherent vacancy-type defects and nano-features present in the ODS alloys, as these can act as strong sinks for lattice defects induced by radiation. The results would contribute to predict the stability of the nano-featured ODS Fe-Cr alloys under the working conditions.

2. Experimental

ODS alloys with target compositions: Fe-14Cr-0.3 Y₂O₃ (wt %), Fe-14Cr-2W-0.3Ti-0.3 Y₂O₃ (wt %) and Fe-14Cr-2W-0.3Ti-0.24Y (wt %), and a non-ODS Fe-14Cr alloy (wt %), were processed by a PM route consisting of MA and consolidation by HIP for 2 h at 1100 °C and 200 MPa. These alloys are hereafter denoted as Fe14CrY, Fe14CrYWTi, Fe14CrWTiY and Fe14Cr, respectively. The processing details are found elsewhere [21-23]. The consolidated billets of Fe14CrY, Fe14CrYWTi and Fe14Cr (~30 mm Ø

×55 mm) were forged between 1050 and 1150 °C into the form of ~12×12×170 mm bars, and afterwards heat treated for 2 h at 850 °C and air cooled. The Fe14CrWTiY alloy was not forged but heat treated for 1 h at 1300 °C. Sample pairs with dimensions 10×10×1 mm were cut by electro-erosion from the ingots, and then their surfaces mechanically polished to a mirror finishing using alumina slurry. The PAS experiments were performed on sample pairs after successive isochronal annealing for 90 min from room temperature and up to 1400 °C in 100 °C steps in a vacuum pressure <10⁻⁵ mbar. The isochronal annealing experiments in the Fe14CrY alloy were performed on three pairs of samples with different starting conditions: as-HIP, as-forged, and heat treated at 850 °C after forging. The starting condition for the Fe14CrYWTi and Fe14Cr alloys was the thermal treatment at 850 °C after forging, and for the Fe14CrWTiY alloy the thermal treatment at 1300 °C.

The positron annihilation experiments were carried out in a fast-fast coincidence spectrometer with a time resolution of 230 ps (FWHM) using a ²²Na source sealed in kapton sandwiched between the pair of samples. Positron lifetime spectra with a total count number >10⁶ were properly fitted to a sum of two lifetime components, τ_1 and τ_2 , after subtracting the corrections due to positron annihilation in the ²²Na source. These spectra are characterized by a mean positron lifetime defined as

$$\langle \tau \rangle = \tau_1 I_1 + \tau_2 I_2 \tag{1}$$

where I_1 and I_2 are intensities of the corresponding components. The instrumental time resolution and contribution of the positron source to the lifetime spectra were determined from measurements on reference samples of annealed pure Fe and Si single crystals. The PATFIT-88 package was used for fitting the spectra [24].

Coincidence Doppler broadening measurements were done using two HP Ge detectors in timing coincidence, placed face to face with the samples at the half-way point between the detectors. The resulting CDB spectrum was the cumulative spectrum of 24 CDB spectra without evidence of electronic shift, each of them with a count number $>10^6$ in a 512×512 coincidence matrix. The cumulative spectra had 1×10^7 counts in the strip centered on the matrix diagonal for the energy range $2m_0c^2 - 1.6$ keV $< E_1 + E_2 < 2m_0c^2 + 1.6$ keV; E_1 and E_2 stand for the energies of the pair of annihilating photons, m_0 the electron rest mass and c the light speed. The spectra were binned from 40 to 512 bins with a bin width of $2.5 \times 10^{-3} m_0c$ to decrease the statistical fluctuations of the data in the high momentum region. The spectra were then normalized and the intensity at a given photon momentum divided by the corresponding counts in the CDB spectrum of a reference sample in order to highlight the differences between the spectra. Pure annealed Fe and Cr, and pure Y_2O_3 were used as reference samples. The fraction of positron annihilating with low- and high-momentum electrons was also measured using the S and W line shape parameters. The S parameter was calculated as the ratio of the count number in the energy window of 1.946 keV centered at 511 keV to the count total in the annihilation peak. The W parameter was calculated as the fraction of counts in the energy interval 515.66 – 519.72 keV and 502.67 – 506.74 keV.

3. Results

3.1. Positron lifetime measurements

The evolution of τ_1 , τ_2 , $\langle \tau \rangle$ and I_2 as a function of annealing temperature is represented in Figures 1 and 2. All the alloys exhibited a two-component spectrum through the annealing temperature range except Fe14CrY in the as-HIP condition, which yielded a single-component after annealing at $950^\circ\text{C} < T < 1350^\circ\text{C}$, see Figure 1a). The lifetime

value of the second component, τ_2 , for Fe14Cr heat treated after forging decays monotonously from ~480 ps to ~360 ps through the temperature range, see Figure 2c). In contrast, the ODS alloys presented a visible recovery of the τ_2 value with onset at temperatures between 750 and 950 °C, which seems to depend on the treatments underwent after their HIP consolidation as the plots represented in Figures 1 and 2 reveal. Up to the recovery temperature, the τ_2 value remained essentially constant for these alloys except for Fe14CrY in the as-forged condition. After annealing at $T < 950$ °C the mean value of τ_2 resulted in (350 ± 40) ps and (293 ± 24) ps for Fe14CrY in the starting conditions as-HIP and heat treated after forging, respectively, (269 ± 9) ps for Fe14CrYWTi heat treated after forging and (291 ± 12) ps for heat treated Fe14CrWTiY. In order to emphasize the changes accompanying the recovery, the dispersion in the I_2 values was limited constraining τ_2 to the mean value above quoted for the corresponding spectra. Short lifetime values, ranging between 110 and ~200 ps in these alloys, may be attributed to positron annihilation at an abundant variety of defects inherent to their complex microstructure such as single vacancies, divacancies or trivacancies, impurity-vacancy complex, dislocations or defects associated with them as jogs, vacancies and impurity-vacancy complexes, defects at grain boundaries and interfaces, as well as defects related with second-phase precipitates [14, 25, 26]. Positron lifetime values between 220 and 400 ps appear to be characteristic of annihilation in tridimensional vacancy clusters or nanovoids in α -Fe [27-29].

In the interpretation of the lifetime results the following remarks have to be considered. 1) The fact that positron lifetime spectra are inconsistent with a standard trapping model derives from the complex microstructure of these alloys as revealed by TEM analyses [22, 23, 30]. The high number density and variety of complex defects, heterogeneously distributed in many cases, prevent any precise and reliable information

about the defects contributing to the short lifetime component even though a diffusion-limited trapping model is applied. 2) Attempts for decomposing the short lifetime component in those spectra that exhibited a τ_1 value as high as ~ 200 ps, increasing the total number count of the spectra or constraining the lifetime values, failed. These analyses resulted in unrealistic lifetime values, or alternatively, either negative or meaningless intensity values with very large errors, and unacceptable variances. The above remarks point out that the second lifetime component that appears in the ODS alloys after annealing at 950°C would be essentially attributable to real changes in the positron traps induced by annealing. Moreover, specific information about the positron traps responsible for the short lifetime component cannot be achieved from the present results. Nevertheless, the partial recovery or transformation of these traps can be inferred from the changes in the lifetime τ_1 and intensity $I_1 = 1 - I_2$.

3.1a. Fe14CrY

Figure 1 summarizes the effect of the thermo-mechanical treatment on the annihilation parameters for the ODS Fe14CrY alloy. The second lifetime of 350 ps, present in the as-HIP condition, disappears completely after annealing at temperatures in the interval $950^\circ\text{C} < T < 1350^\circ\text{C}$ but a very strong second lifetime component of ~ 250 ps develops after annealing at 1350°C . This is observed along with a considerable reduction of the τ_1 value, which indicates thermal activated vacancy release from defects contributing to the short lifetime component and formation of new open-volume defects. The evolution of I_2 indicates the recovery onset of vacancy-type defects at 750°C , which means that the defects responsible for the 350 ps component become unstable and start to release vacancies. These migrating vacancies appear to flow to strong vacancy sinks contributing to the short lifetime component, as its lifetime value rises from (195 ± 2) ps

to (220 ± 1) ps up to developing tridimensional vacancy clusters that give rise to the observed second lifetime component of ~ 250 ps.

The alloy in the as-forged condition exhibits an initial second lifetime component of 260 ps with a much higher intensity I_2 than the one for the alloy in the as-HIP condition, 28% against 1.2%, see the corresponding plots in Figure 1. After annealing at 150 °C, I_2 goes down to 9% and τ_2 increases to ~ 400 ps. These values remain practically constant after the successive anneals up to 750 °C. This indicates that a significant part of the defects responsible for this 260 ps component being smaller in size and very much abundant than those of 350 ps in the as-HIP samples are unstable at 150 °C. It should be noted that the forged material in the air-cooled condition may retain vacancies frozen as complex vacancy clusters. The vacancy release from these defects at 150 °C appears to promote coarsening of other more stable defects, although in competition with other vacancy sinks. The latter may be some of the defects that contribute to the short lifetime as the simultaneous increment in τ_1 and I_1 shows. At $T > 750$ °C the τ_2 and τ_1 values start to recover simultaneously. This can be interpreted as dissolution of the large voids responsible for the ~ 380 ps component and trapping of the released vacancies in some of the defects contributing to short positron lifetime, which turn into tridimensional vacancy clusters, or nanovoids. These clusters with lifetime values of (242 ± 7) ps survive after annealing at 1400 °C, for 90 minutes at least. This interpretation would be compatible with the fact that the $\langle \tau \rangle$ value is unaltered after the recovery of the 380 ps traps, see Figure 1b). As an alternative interpretation one can conceive that defects responsible for the lifetime of ~ 240 developed after annealing at $T > 750$ °C were actually present before but contributing to the short lifetime component. Then, it would be resolved by the fits after annealing out the 380 ps defects. However, if

the number density of the 240 ps defects is unchanged after annealing at $T > 750$ °C the $\langle \tau \rangle$ value should very likely decrease instead of remaining essentially constant.

The unexpected large uncertainty in the I_2 value for the as-forged samples after the isochronal anneal at 850 °C, confirmed repeating the measurements at least 3 times, demanded attention, see Figure 1b). Thus, isothermal annealing experiments at 800 °C and 850 °C were performed on a pair of samples starting from the as-forged and air-cooled condition. The results are summarized in Table 1. After isothermal annealing for 30 min at 800 °C the second lifetime component yields I_2 and τ_2 values of (13 ± 17) % and (265 ± 50) ps, which remain essentially constant after isothermal annealing for 270 min. The subsequent isothermal annealing at 850 °C for 30 min induces a remarkable increase in the I_2 value and in its uncertainty, as well as a reduction in τ_2 . Afterwards, the I_2 and τ_2 values appear to be constant after annealing beyond 90 min. It is worth noticing that the τ_1 value remains constant after isothermal annealing at 800 °C longer than 30 min, but it lowers remarkably after isothermal annealing at 850 °C and becomes again constant when the annealing time is above 90 min. This appears to reproduce the τ_1 behavior at the recovery onset of τ_2 in the as-forged Fe14CrY samples isochronally annealed, as the corresponding plot in Figure 1b) and results in Table 1 show.

The evolution of I_2 for the Fe14CrY samples heat treated after forging exhibits an isochronal annealing behavior very similar to that for the samples in as-HIP condition, except for the vanishing of second lifetime component, as the comparison between the plots in Figure 1 reveals. After annealing at 1050 °C, I_2 rises from 10 to 92 % accompanied by a drop in τ_2 from 293 ± 24 to 218 ± 3 ps. At temperatures above 1050 °C, I_2 decreases and τ_2 increases, ending at values of ~60 % and ~245 ps after the final anneal at 1400 °C, in concordance with the corresponding values for the other two pairs of Fe14CrY samples. In the samples heat treated after forging it is worth noticing the

clear correlation of the onset of the I_2 recovery at 750 °C with the rise of τ_1 , as well as the simultaneous correspondence between the maximum values of I_2 with the minimum τ_1 values, as the plots in Figure 1c) show. This correspondence is also evident in the other two pair of samples although it occurs at different temperatures.

Regarding the evolution of the mean positron lifetime $\langle \tau \rangle$ with isochronal annealing no significant changes are observed for the samples in the as-HIP or as-forged conditions. For the samples heat treated after forging, $\langle \tau \rangle$ appears to slightly rise after annealing at 950 °C remaining constant until 1350 °C, and then decreases just below the initial value.

3.1b. *Fe14CrYWTi and Fe14CrWTiY*

As stated in Section 2, the starting conditions for the samples of these two alloys were different: thermal treatment at 850 °C after forging for Fe14CrYWTi and heat treatment at 1300 °C for Fe14CrWTiY. Nevertheless, either alloys exhibit decrease of the I_2 above 750 °C accompanied by a rise of τ_1 in the same way as the Fe14CrY alloy, see the plots in Figure 2. Afterwards, τ_1 and τ_2 recover in coincidence with a steeply increase in I_2 up to attaining a maximum value after annealing at ~1150 °C. Beyond this temperature, τ_1 and τ_2 are practically constant and the mean lifetime $\langle \tau \rangle$ drops due to the decrease of the intensity I_2 , which implies annealing out of the open volume defects responsible for the second lifetime component being more evident for Fe14CrYWTi.

3.1c. *Fe14Cr*

The recovery characteristics of this non-ODS alloy, heat treated at 850 °C after forging, differ noticeably from those observed for the ODS alloys. The lifetime τ_2 does not exhibit the distinctive steep recovery of the ODS alloys at 800 – 1000 °C but a

gradual reduction starting after annealing above 250 °C as the plots in Figures 1 and 2 reveal. Moreover, the recovery of $\langle \tau \rangle$ occurs at 1050 °C corresponding with the continuous I_2 decrease and a constant τ_1 value. Preceding this recovery, I_2 increases at the same time that the reduction in the τ_1 value occurs for annealing above 750 °C. This is also interpreted as evidence of vacancy release from defects contributing to the first lifetime component and subsequent formation of new voids like it occurs for the ODS alloys. In addition, it appears that Fe14Cr heat treated after forging exhibits an initial I_2 decreases concurrently with a considerable increase of the τ_2 value after annealing at 150 °C. This can be the result of vacancy release from unstable vacancy clusters and their competitive trapping in defects responsible for the first lifetime component, and in stable voids that grow.

3.2. CDB measurements

The characteristics of the ratio CDB curves and their evolution with isochronal annealing are shown for selected annealing temperatures in Figures 3 and 4, along with the ratio curves for the reference samples of the alloying elements and Y_2O_3 . All the CDB curves at a given annealing temperature are normalized to the one for Fe14Cr annealed at the corresponding temperature. No significant changes respect to the Fe14Cr samples are found in the low-momentum region, i.e. for $p_L < 10 \times 10^{-3} m_0 c$, after annealing at temperatures $T < 950$ °C. In this region some changes are evident after annealing at $T \geq 950$ °C, except for the Fe14CrYWTi samples. By contrast, the annealing effect on the high-momentum side of the ratio curves of the ODS alloys is obvious. The remarkable reduction of the positron annihilations with high-momentum electrons, relative to the Fe14Cr alloy, appears to be related to a major contribution of the core electrons of Cr, or other alloying elements such as Y, W, Ti and Si, in the annihilation

events. Nevertheless, the effective changes over the high-momentum side appear not to follow a defined pattern revealing the characteristic signature of a particular alloying element. This result can be interpreted as evidence for competitive positron trapping in defects with a configurational surrounding that can either concurrently or separately contain Cr, Y and other alloying impurities.

Figure 5 shows the W - S correlation plots for all the samples. These plots are useful for revealing the presence of different positron traps or changes in the chemical surrounding of the positron annihilation sites during isochronal annealing. It is known in the case of positron annihilation taking place in two positron states, i.e. in a free state and in a trapped state in a single type of defect, or otherwise in two trapped state in two different types of defect, the measured line shape parameters S and W are given by [31]

$$\begin{aligned} S &= f_1 S_1 + (1 - f_1) S_2 \\ W &= f_1 W_1 + (1 - f_1) W_2 \end{aligned} \quad (2)$$

where S_i stand for the line shape parameters representative of the annihilations with the low momentum valence electrons for each state, and W_i the corresponding with the high momentum electrons. From Equation 2 the following correlation is found

$$W = -RS + (W_2 + RS_2) \quad (3)$$

where R is a constant defect specific parameter independent of the number density of positron traps given by

$$R = \frac{W_1 - W_2}{S_2 - S_1} = \frac{W - W_2}{S_2 - S} \quad (4)$$

and the measured values of S and W are in the range $S_1 < S < S_2$ and $W_2 < W < W_1$. Then, if the W - S plot exhibits a full linear dependence, either a single type of defect acts

as positron traps or there exists positron trapping saturation in two effective defects through the recovery and isochronal annealing. This is the case for non-ODS Fe14Cr, see the corresponding plot in Figure 5. In contrast, the plots for the ODS alloys only exhibit a linear dependence after annealing at $T > 1150$ °C except for Fe14CrWTiY heat treated at 1300 °C.

4. Discussion

4.1. Fe14CrY

4.1a. As-forged samples

Among the different samples investigated, it is expected that the ODS Fe14Cr samples in the as-forged condition achieve the most far out of equilibrium microstructure because of the fast cooling rate after forging at 1100 °C. The large increase of τ_2 simultaneously with the significant drop of I_2 after annealing at 150 °C reveals thermal shrinking of metastable vacancy clusters and coarsening of stable ones via trapping of migrating vacancies. These large tridimensional clusters or voids are thermally stable up to 750 °C. Above this temperature these voids become unstable, the representative positron lifetime τ_2 for the voids drops steeply and the intensity I_2 rises simultaneously, see Figure 1b). This can only be interpreted as a sign of development of new vacancy clusters at the expenses of the vacancies released from unstable voids during their thermal shrinkage. The characteristic τ_2 value for the new clusters results to be 235 ± 10 ps after annealing at $T \geq 950$ °C. The fact that the W - S plot for these samples exhibits a constant R value of 0.2330 ± 0.0010 for annealing temperatures $T > 1150$ °C concurrent with the constant value of τ_2 supports the above interpretation. These clusters, as well as those appearing in the temperature range 150 – 750 °C, must be associated with some

solute impurities that stabilize them in the corresponding temperature range. According with the calculi of the positron lifetime for tridimensional vacancy clusters in pure α -Fe, these clusters could contain a number of 3 to 5 vacancies if solute impurities are not found associated with them [25, 26], but they would be unstable at 150 °C [22]. Some impurities would therefore have to be associated with the stable vacancy clusters. Hence, the binding of solute atoms to these clusters would be reflected on the high-momentum region of the CDB spectrum by the contribution of core electrons from the solute atoms. After any annealing step, the high-momentum region of the CDB curves for Fe14CrY in the as-forged condition seems to exhibit characteristics compatible with both the Cr and Y signature, see Figure 3. No conclusive evidence for the association of vacancy clusters with an exclusive atom, i.e. either Cr or Y atoms, can be attained from these curves. Thus, the changes in the high-momentum region induced by successive isochronal annealing can be interpreted as the result of the concurrent contribution of core electrons from Cr and Y atoms associated with the positron traps.

4.1b. Heat-treated samples after forging

The effect of the heat treatment at 850 °C after forging is to shift the edge of the abrupt changes in I_2 , τ_2 and τ_1 from 750 °C to 950 °C, see Fig 1c). Nevertheless, these changes are preceded by a recovery of I_2 and a rise of τ_1 indicating that: 1) some unstable vacancy clusters still remain after the pre-treatment at 850 °C for 2 h, and 2) there exists a flow of the vacancies released from the shrinking clusters to some defects that contributes to the first lifetime component, as occurs for the samples annealed in the as-forged condition. These defects would have capability for trapping vacancies giving rise to a variety of positron traps apparently stable at 1050 °C. Above this temperature, I_2 decreases rapidly with a simultaneous increase of τ_2 , which suggests shrinkage of some

clusters and coarsening of others. However, the last anneal at 1400 °C lowers considerably the τ_2 , τ_1 and $\langle \tau \rangle$ values revealing unstability of the defects, see Figure 1c). In these samples the linear correlation between the parameters W and S is also apparent after annealing at $T > 1150$ °C with a parameter R of 0.2590 ± 0.0021 as the corresponding plot in Figure 5 reveals. For annealing at $T \leq 1150$ °C the W and S values are found apparently randomly distributed in a bound region suggesting a complex annihilation scheme in the samples with positron annihilations in more than two states. In contrast, this concentration of the W and S values does not occur for the as-forged samples. This difference in the evolution of the parameters W and S can be attributed to the pre-treatment at 850 °C.

The comparison of the ratio CDB spectra with those for the as-forged samples reveals that the fast recovery of I_2 after annealing at $T > 1150$ °C is related to a considerable reduction of the Cr and Y contribution to high-momentum annihilations, see Figure 3. The above and the fact that the defects induced by annealing at 1050 °C are clearly unstable at higher temperatures in the heat treated samples, in parallel with the significant drop of $\langle \tau \rangle$ after annealing at 1400 °C, would indicate a relationship between the thermal stability of the defects and the presence of Y and Cr atoms in their surroundings.

4.1c. As-HIP samples

These samples through isochronal annealing at $T \leq 950$ °C replicate the evolution of the positron lifetime parameters observed in the samples heat treated after forging, see Figure 1. Now, I_2 for $T \leq 950$ °C is considerably smaller, and τ_2 and τ_1 larger, than the corresponding values for the samples heat treated after forging. However, it is worth to notice that in any case the $\langle \tau \rangle$ values for the Fe14CrY alloy coincide just at the starting

of the isochronal annealing experiments irrespective of the previous thermo-mechanical treatment. This result reveals that the HIP consolidated ODS Fe14Cr alloy contains an effective concentration of positron traps high enough to attain trapping saturation despite the subsequent treatments herein applied.

At temperatures above 950 °C, the vacancy clusters responsible for the lifetime component of 350 ps anneal out, and a single lifetime component emerges gradually increasing its lifetime up to a value of 220 ± 1 ps upon annealing at 1250 °C. It is worth to be aware that the lifetime of the vacancy clusters growing after annealing at 1050 °C is 218 ± 3 ps in the samples heat-treated after forging and 221 ± 3 in the as-forged samples. Then, the single lifetime component of 220 ps appears to be due to positron annihilation saturation in the vacancy clusters grown by annealing, which coarsen at $T > 1250$ °C while their concentration declines as the plot in Figure 1a) reflects. This interpretation is supported by the corresponding W - S plots in Figure 5. Now, in opposition to that occurring for the other two Fe14CrY samples the lineal W dependence on S for $T > 1150$ °C is decreasing with annealing temperature resulting in a defect specific parameter R of 0.349 ± 0.019 . Furthermore, the random evolution of the data points through isochronal annealing at $T \leq 1150$ °C reflects a starting defect structure in these samples that differs from those in the other two pair samples thermo-mechanically treated.

4.2. Fe14CrYWTi heat-treated samples after forging

The evolution of the lifetime parameters with isochronal annealing for these samples exhibits significant coincidences with the ODS Fe14Cr samples submitted to the same thermo-mechanical treatment as the respective plots in Figures 1c) and 2a) reveal. These are: 1) the I_2 recovery onset above 750 °C and simultaneous increase of τ_1 , and 2) the

development of new vacancy clusters at $T > 950$ °C revealed by the abrupt rise of I_2 concurrently with a considerable drop in τ_1 and τ_2 . By contrast, there exist evident differences: 1) at $T > 1150$ °C, a remarkable recovery of the mean positron lifetime $\langle \tau \rangle$ appears with its onset at 1150 °C while the τ_1 and τ_2 values remain practically constant; and 2) at $T < 1050$ °C, the second lifetime component due to vacancy clusters yield I_2 values at least ~ 2.5 times higher than those for the Fe14CrY samples, and τ_2 values considerably smaller, i.e. 270 ps against 292 ps. These noteworthy differences respect to the counterpart Fe14CrY samples can only be attributed to the W and Ti addition. Nevertheless, a linear relationship between W and S like the one for the Fe14CrY samples is satisfied after annealing at $T > 1150$ °C with a parameter $R = 0.322 \pm 0.006$, see the plots in Figure 5. For annealing at $T \leq 1150$ °C the parameters W and S are found bounded inside an interval of values even narrower than the one for the counterpart pair of Fe14CrY samples being also attributable to the effect of the heat treatment at 850 °C after forging. As the I_2 value scales with the number concentration of the vacancy-type defects responsible for this lifetime component, and τ_2 does it with the size, the positron lifetime results indicate that either W or Ti promotes the formation and refinement of the vacancy clusters. Since TEM studies of ODS Fe14CrWTi have revealed the capability of Ti for improving the dispersion of oxide particle via its incorporation into the oxide particle [32], the aforementioned differences should accordingly be associated with the Ti effect on the dispersion.

4.3. Fe14CrWTiY heat-treated at 1300 °C

The changes in the lifetime parameters for these samples are qualitatively similar to those found in Fe14CrYWTi as the plots in Figure 2 show, even though the respective pre-treatments were very different. A small recovery stage of I_2 at $T > 750$ °C followed

by a strong rise of I_2 , and a second recovery at $T > 1150^\circ\text{C}$ appear, which are accompanied by qualitative changes in τ_2 , τ_1 and $\langle \tau \rangle$ similar to those observed in the Fe14CrYWTi samples. The fact that the I_2 values after annealing at $T \leq 750^\circ\text{C}$ are a factor of ~ 1.5 to 2 smaller than the ones for Fe14CrYWTi may be attributed to annealing induced by the pre-treatment at 1300°C for 1 h. But, it should be noted that after the final isochronal anneals at 1350°C and 1400°C , which were longer in time than the pre-treatment for Fe14CrYWTi, I_2 and $\langle \tau \rangle$ for Fe14CrWTiY stay at values significantly higher than those for Fe14CrYWTi, i.e. 50 % and 200 ps against 40 % and 170 ps. This result is compatible with a possible presence of defects more stable than the ones present in Fe14CrYTiW. This possibility is supported by the TEM analyses accomplished in these samples that evidence a clear effect of the unintentional Si impurities on the oxide dispersion characteristics developed [21]. It was found that complex Y-Si oxide nanoparticles developed predominantly instead of Y-Ti oxide dispersoids. In that case, the high stability of vacancy clusters in these samples might be attributed to their association with the Y-Si oxide dispersoids or Si solutes.

The W - S plot for Fe14CrWTiY exhibits a clear difference respect to those for the other ODS alloys, see Figure 5. The transition to a linear correlation between W and S after annealing at $T > 1150^\circ\text{C}$ is no longer evident, being very likely attributable to the pre-treatment at 1300°C . As a result the W and S values appear not to be correlated with the annealing temperature over the whole temperature range. This means that the nano-features resulting in these samples is more complex than those for the other ODS alloys, which could be attributed to the effect of Si impurities present in these samples according with the above discussion. As occurs in the Fe14CrY alloy, the ratio CDB spectra shown in Figure 4 do not exhibit any clear sign attributable to any of the alloying impurities over the whole range of annealing temperature. The ratio CDB

curves for reference samples of Si is also represented in Figure 4 to assess the Si effect on the enhanced stability of the vacancy clusters in the Fe₁₄CrW₁TiY alloy unintentionally contaminated with Si. Moreover, the shape and evolution of the high-momentum side of the spectra being quite similar to the ones for Fe₁₄CrY suggest a minor participation of the core electrons from W, Ti and Si in the positron annihilations. At present, a consistent explanation of the enhanced stability of the vacancy defects developed in the Fe₁₄CrW₁TiY samples cannot be given except that it is likely due to the thermo-mechanical treatments underwent by the samples.

5. Conclusions

Positron annihilation measurements were performed on samples of the ODS Fe₁₄Cr and Fe₁₄CrW₁Ti alloys submitted to sequential isochronal annealing. The main findings are summarized as follows:

- (1) Irrespective of the starting conditions of the samples, the results revealed the presence of tridimensional vacancy clusters, or defect nano-features, some of which can survive annealing at 1400 °C for 90 min, at least.
- (2) The evolution of the positron annihilation characteristics shows two recovery stages for these vacancy type defects. The first one starting at $T > 750$ °C is attributed to thermal shrinkage of large vacancy clusters, or voids, and consequent trapping of the released vacancies by other defects of different nature.
- (3) Annealing in the temperature interval $800 < T \leq 1050$ °C gives rise to new vacancy clusters, whose number concentration is considerably higher than the one for the vacancy clusters existing at $T \leq 750$ °C. The new vacancy clusters start to anneal out at $T > 1050$ °C in the Fe₁₄CrY samples and at $T > 1150$ °C in Fe₁₄CrYWTi

and Fe₁₄CrW₁TiY. In the case of the Fe₁₄CrY samples isochronally annealed starting from the as-forged condition, the new clusters appear to exhibit the highest thermal stability.

- (4) The number concentration of the vacancy clusters present in the Fe₁₄CrYWTi samples after annealing at $T \leq 750$ °C is considerable higher, and their size smaller, compared with the corresponding ones in the Fe₁₄CrW₁TiY samples. However, the major part of vacancy defects developed upon annealing at ~950 °C result to be remarkably more stable in Fe₁₄CrW₁TiY than in Fe₁₄CrYWTi.
- (5) The W-S plots for the ODS Fe₁₄Cr and Fe₁₄CrYWTi alloys reveal a clear transition in the relationship between these parameters after annealing at temperatures above 1050 °C. This is compatible with a change in the structure of the nano-features present in these alloys. This transition is not present in non-ODS Fe₁₄Cr alloys or in the case of the ODS Fe₁₄CrW₁TiY alloy pre-heated at 1300 °C.

Acknowledgments

This investigation was supported by the Spanish Ministry of Economy and Competitiveness (project ENE2012-39787-C06-05), Comunidad de Madrid (Spain) through the MULTIMATCHALLENGE (S2013/MIT-2862) and TECHNOFUSION (II)-CM (S2013/MAE-2745) programs, and European Commission through the European Fusion Development Agreement (contracts 09-240 and 10-425).

References

[1] S. Ukai, and M. Fujiwara, J Nucl Mater, 307 (2002) 749-757.
[2] L.K. Mansur, A.F. Rowcliffe, R.K. Nanstad, S.J. Zinkle, W.R. Corwin, and R.E. Stoller, J Nucl Mater, 329 (2004) pp. 166-172.
[3] K.L. Murty, and I. Charit, J Nucl Mater, 383 (2008) pp. 189-195.

- [4] G.R. Odette, M.J. Alinger, and B.D. Wirth, *Annu Rev Mater Res*, 38 (2008) pp. 471-503.
- [5] D.J. Larson, P.J. Maziasz, I.S. Kim, and K. Miyahara, *Scripta Mater*, 44 (2001) pp. 359-364.
- [6] V. de Castro, E.A. Marquis, S. Lozano-Perez, R. Pareja, and M.L. Jenkins, *Acta Mater*, 59 (2011) pp. 3927-3936.
- [7] M.K. Miller, and C.M. Parish, *Mater Sci Tech-Lond*, 27 (2011) pp. 729-734.
- [8] A. Hirata, T. Fujita, Y.R. Wen, J.H. Schneibel, C.T. Liu, and M.W. Chen, *Nat Mater*, 10 (2011) pp. 922-926.
- [9] C.A. Williams, P. Unifantowicz, N. Baluc, G.D.W. Smith, and E.A. Marquis, *Acta Mater*, 61 (2013) pp. 2219-2235.
- [10] C.A. Williams, G.D.W. Smith, and E.A. Marquis, *Scripta Mater*, 67 (2012) 108-111.
- [11] P. He, M. Klimenkov, R. Lindau, and A. Moslang, *J Nucl Mater*, 428 (2012) pp. 131-138.
- [12] T. Liu, H. Shen, C. Wang, and W. Chou, *Mater Res Innov*, 18 (2014) pp. 410-413.
- [13] Z.H. Yao, W.H. Xiong, G.P. Zhang, X. Chen, and B. Huang, *Mater Design*, 56 (2014) pp. 953-958.
- [14] Y. Ortega, V. de Castro, M.A. Monge, A. Munoz, T. Leguey, and R. Pareja, *J Nucl Mater*, 376 (2008) pp. 222-228.
- [15] J. Xu, C.T. Liu, M.K. Miller, and H.M. Chen, *Phys Rev B*, 79 (2009).
- [16] Y. Ortega, M.A. Monge, V. de Castro, A. Munoz, T. Leguey, and R. Pareja, *J Nucl Mater*, 386-88 (2009) pp. 462-465.
- [17] R. Pareja, P. Parente, A. Munoz, A. Radulescu, and V. de Castro, *Philos Mag*, 95 (2015) pp. 2450-2465.
- [18] R.W. Siegel, *Annu Rev Mater Sci*, 10 (1980) pp. 393-425.
- [19] M.J. Puska, and R.M. Nieminen, *Rev Mod Phys*, 66 (1994) pp. 841-897.
- [20] P. AsokaKumar, M. Alatalo, V.J. Ghosh, A.C. Kruseman, B. Nielsen, and K.G. Lynn, *Phys Rev Lett*, 77 (1996) pp. 2097-2100.
- [21] M.A. Auger, T. Leguey, A. Munoz, M.A. Monge, V. de Castro, P. Fernandez, G. Garces, and R. Pareja, *J Nucl Mater*, 417 (2011) pp. 213-216.
- [22] M.A. Auger, V. de Castro, T. Leguey, M.A. Monge, A. Munoz, and R. Pareja, *J Nucl Mater*, 442 (2013) S142-S147.

[23] M.A. Auger, V. de Castro, T. Leguey, J. Tarcisio-Costa, M.A. Monge, A. Munoz, and R. Pareja, *J Nucl Mater*, 455 (2014) pp. 600-604.

[24] P. Kirkegaard, N.J. Pedersen, and M. Eldrup, *Risø Report M2740*, Risø National Laboratory, Denmark, (1989).

[25] A. Vehanen, P. Hautojarvi, J. Johansson, J. Ylikauppila, and P. Moser, *Phys Rev B*, 25 (1982) pp. 762-780.

[26] V. Krsjak, Z. Szaraz, and P. Hahner, *J Nucl Mater*, 428 (2012) pp. 160-164.

[27] M.J. Puska, and R.M. Nieminen, *J Phys F Met Phys*, 13 (1983) pp. 333-346.

[28] H. Ohkubo, Z. Tang, Y. Nagai, M. Hasegawa, T. Tawara, and M. Kiritani, *Mat Sci Eng A-Struct*, 350 (2003) pp. 95-101.

[29] J. Kuriplach, O. Melikhova, C. Domain, C.S. Becquart, D. Kulikov, L. Malerba, M. Hou, A. Almazouzi, C.A. Duque, and A.L. Morales, *Appl Surf Sci*, 252 (2006) pp. 3303-3308.

[30] M.A. Auger, T. Leguey, V. de Castro, M.A. Monge, and R. Pareja, *Mater Sci Tech-Lond*, 30 (2014) pp. 1704-1708.

[31] X. Wu, K.R. Hebert, P. Asoka-Kumar, and K.G. Lynn, *J. Electrochem. Soc.*, 141 (1994) pp. 3361-3368.

[32] A. Hirata, T. Fujita, C.T. Liu, and M.W. Chen, *Acta Mater*, 60 (2012) pp. 5686-5696.

Table 1: Isothermal annealing effect on the positron lifetime spectrum of as-forged Fe14CrY.

Fe14CrY	Annealing time (min)	τ_1 (ps)	τ_2 (ps)	I_2 (%)	$\langle \tau \rangle$ (ps)
As-forged	---	180±7	256±16	29±12	202±60
+ Annealed at 800 °C	30	189±8	265±50	13±17	199±80
	90	188±7	273±40	13±12	199±60
	270	188±6	278±40	13±11	200±60
+ Annealed at 850 °C	30	154±50	217±22	70±50	204±200
	90	120±30	209±3	89±7	199±20
	270	119±13	217±3	80±4	197±18

1
2
3
4
5
6
7
8
9
10
11
12
13
14
15
16
17
18
19
20
21
22
23
24
25
26
27
28
29
30
31
32
33
34
35
36
37
38
39
40
41
42
43
44
45
46
47
48
49
50
51
52
53
54
55
56
57
58
59
60

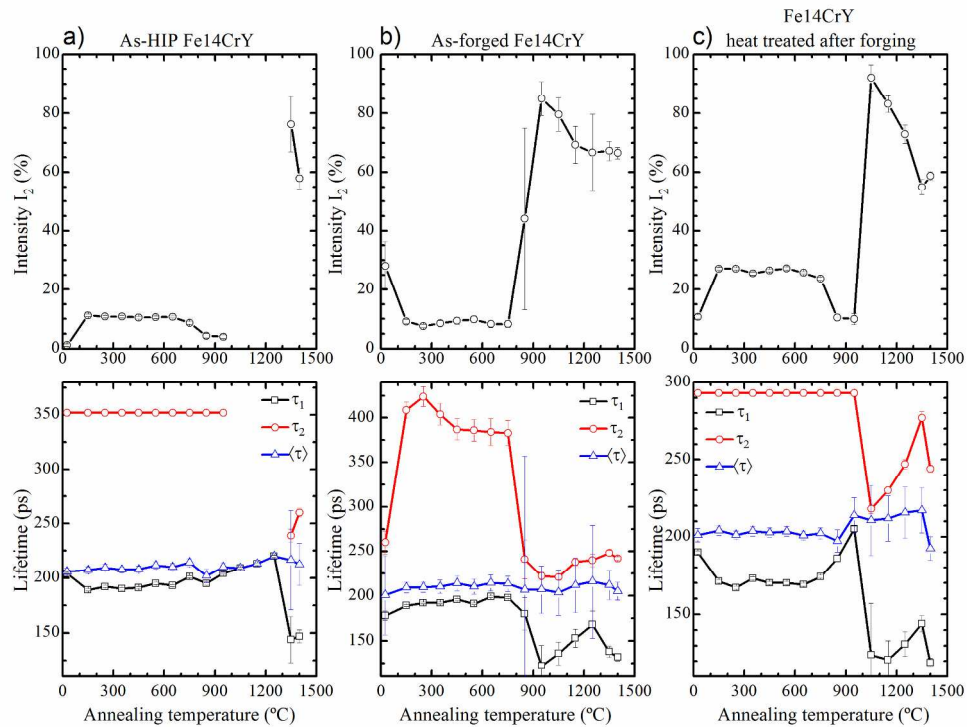
Figure 1. Isochronal annealing effect on the positron lifetime parameters for the ODS Fe14Cr alloy (Fe14CrY) in different conditions: a) as-HIP, b) as-forged and c) heat treated after forging.

Figure 2. Isochronal annealing effect on the positron lifetime parameters for the alloys: a) Fe14CrYWTi heat treated at 850 °C after forging, b) Fe14CrWTiY heat treated at 1300 °C and c) non-ODS Fe14Cr heat treated at 850 °C after forging.

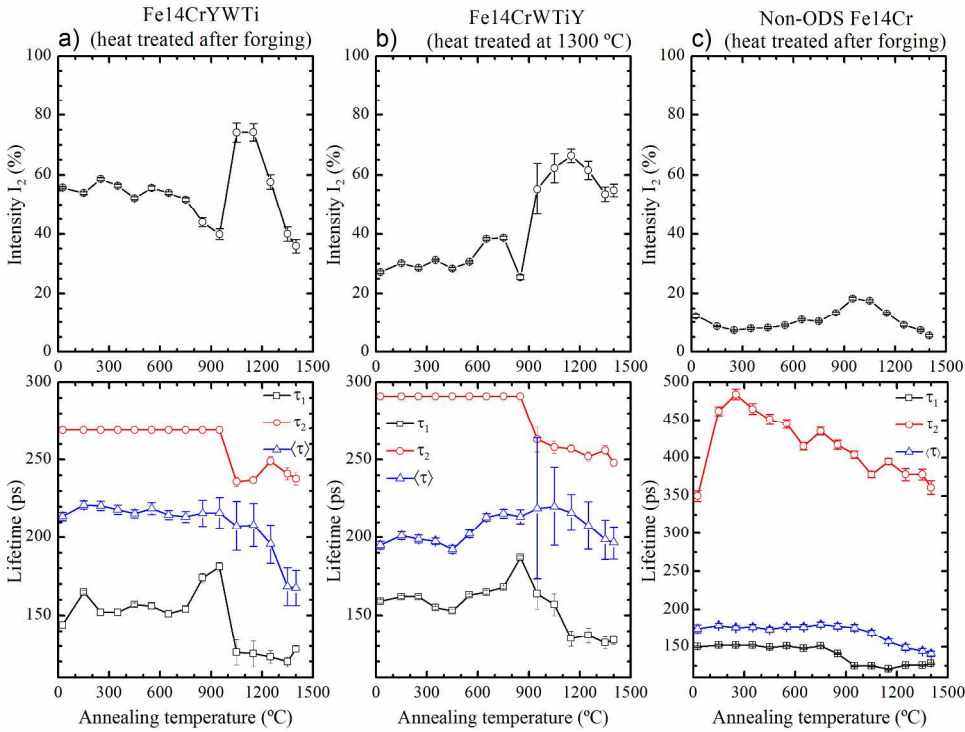
Figure 3. CDB ratio spectra for the ODS Fe14CrY alloy isochronally annealed at different temperatures. The starting conditions of the samples were (-●-) as-HIP, (-■-) as-forged and (-▲-) heat treated at 850 °C after forging. The CDB ratio curves for Fe, Cr and Y₂O₃ are shown for comparison.

Figure 4. Isochronal annealing effect on the CDB ratio spectra for (-●-) Fe14CrYWTi heat treated at 850 °C after forging, and (-■-) Fe14CrWTiY heat treated at 1300 °C. The CDB ratio curves for Fe, Cr, W, Ti, Si and Y₂O₃ oxide are shown for comparison.

Figure 5. S-W plots obtained from CDB data for the ODS and non-ODS Fe14Cr alloys isochronally annealed.

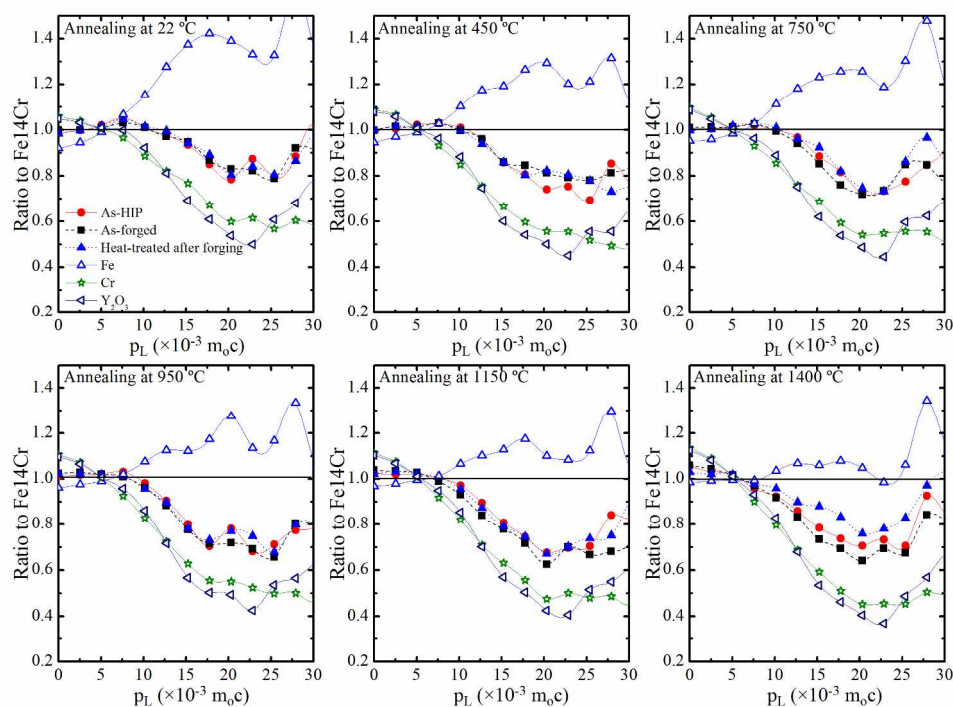


Isochronal annealing effect on the positron lifetime parameters for the ODS Fe14Cr alloy (Fe14CrY) in different conditions: a) as-HIP, b) as-forged and c) heat treated after forging.
239x182mm (300 x 300 DPI)



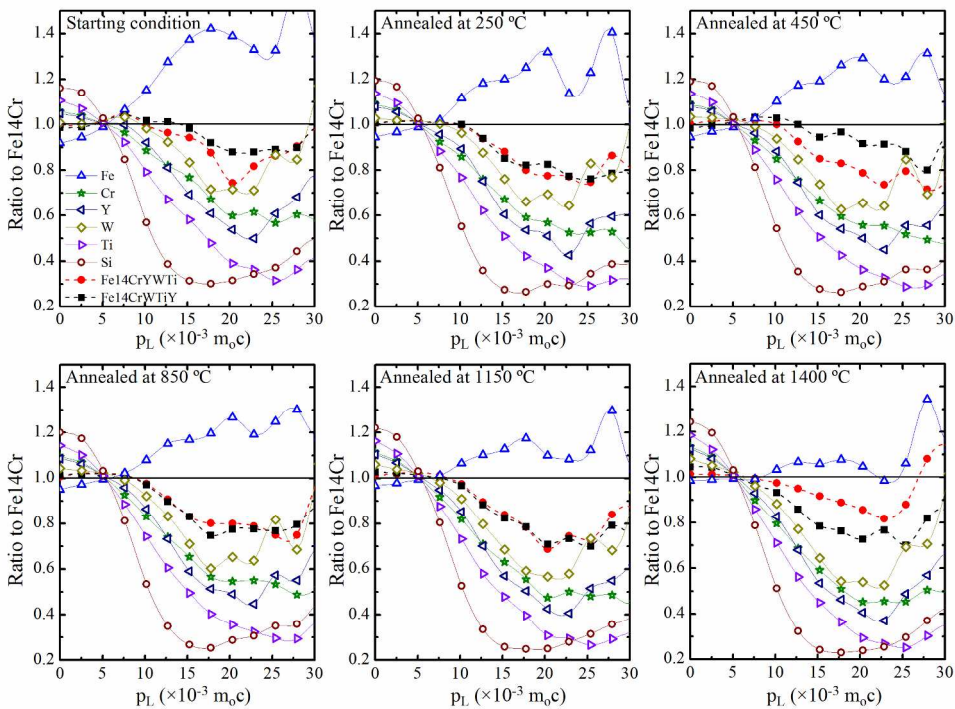
Isochronal annealing effect on the positron lifetime parameters for the alloys: a) Fe14CrYWTi heat treated at 850 °C after forging, b) Fe14CrWTiY heat treated at 1300 °C and c) non-ODS Fe14Cr heat treated at 850 °C after forging.

238x178mm (300 x 300 DPI)

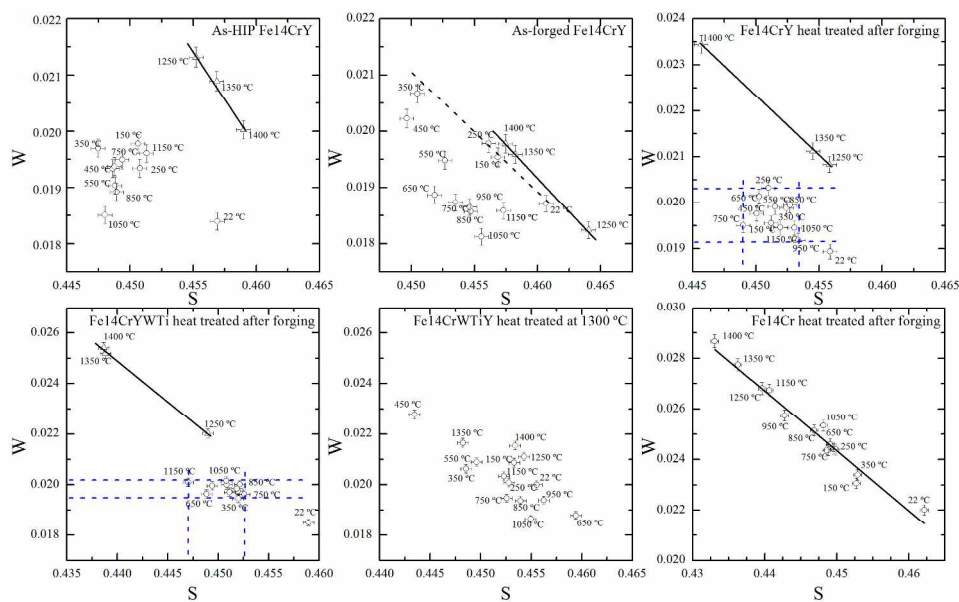


CDB ratio spectra for the ODS Fe14CrY alloy isochronally annealed at different temperatures. The starting conditions of the samples were (-●-) as-HIP, (-■-) as-forged and (-▲-) heat treated at 850 °C after forging. The CDB ratio curves for Fe, Cr and Y2O3 are shown for comparison.

238x176mm (300 x 300 DPI)



Isochronal annealing effect on the CDB ratio spectra for (-●-) Fe14CrYWTi heat treated at 850 °C after forging, and (-■-) Fe14CrWTiY heat treated at 1300 °C. The CDB ratio curves for Fe, Cr, W, Ti, Si and Y2O3 oxide are shown for comparison.
238x175mm (300 x 300 DPI)



S-W plots obtained from CDB data for the ODS and non-ODS Fe14Cr alloys isochronally annealed.
240x152mm (300 x 300 DPI)

1
2
3
4
5
6
7
8
9
10
11
12
13
14
15
16
17
18
19
20
21
22
23
24
25
26
27
28
29
30
31
32
33
34
35
36
37
38
39
40
41
42
43
44
45
46
47
48
49
50
51
52
53
54
55
56
57
58
59
60

Table 1: Isothermal annealing effect on the positron lifetime spectrum of as-forged Fe14CrY.

Fe14CrY	Annealing time (min)	τ_1 (ps)	τ_2 (ps)	I_2 (%)	$\langle \tau \rangle$ (ps)
As-forged	---	180±7	256±16	29±12	202±60
+ Annealed at 800 °C	30	189±8	265±50	13±17	199±80
	90	188±7	273±40	13±12	199±60
	270	188±6	278±40	13±11	200±60
+ Annealed at 850 °C	30	154±50	217±22	70±50	204±200
	90	120±30	209±3	89±7	199±20
	270	119±13	217±3	80±4	197±18

Positron annihilation study of the vacancy clusters in ODS Fe-14Cr alloys

R. Domínguez-Reyes^{a*}, M. A. Auger^{a,b}, M. A. Monge^a and R. Pareja^a

^a*Departamento de Física, Universidad Carlos III de Madrid, Avda. de la Universidad 30. 28911 Leganés, Madrid, Spain.*

^b*Department of Materials, University of Oxford. OX1 3PH Oxford, UK.*

* Corresponding author. E-mail address: rdomingu@fis.uc3m.es (R. Domínguez-Reyes)

Positron annihilation study of the vacancy clusters in ODS Fe-14Cr alloys

Oxide dispersion strengthened Fe14Cr and Fe14CrWTi alloys produced by mechanical alloying and hot isostatic pressing were subjected to isochronal annealing up to 1400 °C, and the evolution and thermal stability of the vacancy type defects were investigated by positron annihilation spectroscopy. The results were compared to those from a non-oxide dispersion strengthened Fe14Cr alloy produced by following the same powder metallurgy route. The long lifetime component of the positron annihilation spectra revealed the existence of tridimensional vacancy clusters, or nanovoids, in all these alloys. Two recovery stages are found in the oxide dispersion strengthened alloys irrespective of the starting conditions of the samples. The first one starting at $T > 750$ °C is attributed to thermal shrinkage of large vacancy clusters, or voids. A strong increase in the intensity of the long lifetime after annealing at temperatures in the 800 - 1050 °C range indicates the development of new vacancy clusters. These defects appear to be unstable above 1050 °C, but some of them remain at temperatures as high as 1400 °C, at least for 90 min.

Keywords: word; positron annihilation, steel, ODS alloys, vacancy clusters

1. Introduction

Dispersion strengthened ferritic Fe-Cr alloys with Y_2O_3 addition are presently considered one of the most promising structural materials for the future fusion reactors and generation IV fission reactors due to their enhanced high temperature strength, microstructural stability, radiation resistance, and good creep resistance at high temperature [1-4]. The appropriate powder metallurgy processing of these alloys develops a homogeneous dispersion of nano-sized hard particles that governs these mandatory properties. Analytical transmission electron microscopy (TEM) and atom probe tomography (APT) studies have contributed to reveal the dimensional, structural and compositional characteristics of the nanoparticles present in these alloys [5-9]. The

fundamental elements of these nano-features are O, Y and Cr, and some alloying impurities intentionally or accidentally added such as Ti, Al or Si [10-13], which appear to refine the size and increase the number density and stability of these nano-features. Experimental evidences for defective nanoclusters, or nano-features, in the ODS steel with a nominal composition Fe-14Cr-3.0W-0.4Ti-0.24Y₂O₃ (wt%), denoted as 14YWTi, have been found from analytical and high resolution transmission electron microscopy (TEM) studies [8]. There are also positron annihilation spectroscopy (PAS) results that point out certain association between vacancy clusters, or nanovoids, and the oxide dispersion in ODS steels [14-16]. It should be noticed that there are PAS results showing vacancy clustering, as well the opposite, in non-ODS steels processed following a powder metallurgy (PM) route similar to the ODS ones, i.e. mechanical alloying (MA) and hot isostatic pressing (HIP) consolidation [14, 17]. It is the case of the non-ODS steels with nominal composition Fe-12wt%Cr showing no evidence of tridimensional vacancy clusters in the as-HIP condition, but these clusters were detected after a heat treatment at 850 °C [17]. These results suggest that the designedly addition of solutes such as Y and Ti would not be the decisive factors for vacancy clustering associated to the oxide nano-features in the ODS steels but the processing conditions and the thermal history of the alloy.

To evidence the above and provide a better understanding on the role of the vacancies in the formation of nano-features in the ODS steels, and on the vacancy cluster behavior, a series of comprehensive isochronal annealing experiments and PAS measurements have been accomplished in ODS Fe14Cr alloys, with and without (W+Ti) addition, and in the counterpart non-ODS Fe14Cr alloy. PAS is a successful technique to study vacancy-type defects in metals and alloys [18]. Lattice defects such as vacancies, voids, solute-vacancy complexes and other open-volume defects are

effective traps for thermalized positrons in a solid. When a positron annihilates trapped in a defect, the annihilation radiation conveys information about the defect. The positron lifetime distribution provides information on the type, size and concentration of the defects. In addition, the Doppler broadening of the annihilation radiation peak at 511 keV, which depends on the momentum of the electrons annihilating with the thermalized positrons, can give information about the chemical surround of the positron annihilation sites [19, 20]. Thus, the concurrent positron lifetime spectroscopy (PLS) and coincidence Doppler broadening (CDB) measurements in isochronally annealed samples would contribute to assess the recovery kinetics of the vacancy defects and their stability in relation with the solute impurities in the ODS alloys. The understanding and assessment of these subjects are of prime interest for developing irradiation-resistant and high-temperature alloys for structural applications. The stability and recovery of radiation-induced defects would be associated with the inherent vacancy-type defects and nano-features present in the ODS alloys, as these can act as strong sinks for lattice defects induced by radiation. The results would contribute to predict the stability of the nano-featured ODS Fe-Cr alloys under the working conditions.

2. Experimental

ODS alloys with target compositions: Fe-14Cr-0.3 Y₂O₃ (wt %), Fe-14Cr-2W-0.3Ti-0.3 Y₂O₃ (wt %) and Fe-14Cr-2W-0.3Ti-0.24Y (wt %), and a non-ODS Fe-14Cr alloy (wt %), were processed by a PM route consisting of MA and consolidation by HIP for 2 h at 1100 °C and 200 MPa. These alloys are hereafter denoted as Fe14CrY, Fe14CrYWTi, Fe14CrWTiY and Fe14Cr, respectively. The processing details are found elsewhere [21-23]. The consolidated billets of Fe14CrY, Fe14CrYWTi and Fe14Cr (~30 mm Ø

×55 mm) were forged between 1050 and 1150 °C into the form of ~12×12×170 mm bars, and afterwards heat treated for 2 h at 850 °C and air cooled. The Fe₁₄CrW₂TiY alloy was not forged but heat treated for 1 h at 1300 °C. Sample pairs with dimensions 10×10×1 mm were cut by electro-erosion from the ingots, and then their surfaces mechanically polished to a mirror finishing using alumina slurry. The PAS experiments were performed on sample pairs after successive isochronal annealing for 90 min from room temperature and up to 1400 °C in 100 °C steps in a vacuum pressure <10⁻⁵ mbar. The isochronal annealing experiments in the Fe₁₄CrY alloy were performed on three pairs of samples with different starting conditions: as-HIP, as-forged, and heat treated at 850 °C after forging. The starting condition for the Fe₁₄CrYWTi and Fe₁₄Cr alloys was the thermal treatment at 850 °C after forging, and for the Fe₁₄CrW₂TiY alloy the thermal treatment at 1300 °C.

The positron annihilation experiments were carried out in a fast-fast coincidence spectrometer with a time resolution of 230 ps (FWHM) using a ²²Na source sealed in kapton sandwiched between the pair of samples. Positron lifetime spectra with a total count number >10⁶ were properly fitted to a sum of two lifetime components, τ_1 and τ_2 , after subtracting the corrections due to positron annihilation in the ²²Na source. These spectra are characterized by a mean positron lifetime defined as

$$\langle \tau \rangle = \tau_1 I_1 + \tau_2 I_2 \quad (1)$$

where I_1 and I_2 are intensities of the corresponding components. The instrumental time resolution and contribution of the positron source to the lifetime spectra were determined from measurements on reference samples of annealed pure Fe and Si single crystals. The PATFIT-88 package was used for fitting the spectra [24].

Coincidence Doppler broadening measurements were done using two HP Ge detectors in timing coincidence, placed face to face with the samples at the half-way point between the detectors. The resulting CDB spectrum was the cumulative spectrum of 24 CDB spectra without evidence of electronic shift, each of them with a count number $>10^6$ in a 512×512 coincidence matrix. The cumulative spectra had 1×10^7 counts in the strip centered on the matrix diagonal for the energy range $2m_0c^2 - 1.6$ keV $< E_1 + E_2 < 2m_0c^2 + 1.6$ keV; E_1 and E_2 stand for the energies of the pair of annihilating photons, m_0 the electron rest mass and c the light speed. The spectra were binned from 40 to 512 bins with a bin width of $2.5 \times 10^{-3} m_0c$ to decrease the statistical fluctuations of the data in the high momentum region. The spectra were then normalized and the intensity at a given photon momentum divided by the corresponding counts in the CDB spectrum of a reference sample in order to highlight the differences between the spectra. Pure annealed Fe and Cr, and pure Y_2O_3 were used as reference samples. The fraction of positron annihilating with low- and high-momentum electrons was also measured using the S and W line shape parameters. The S parameter was calculated as the ratio of the count number in the energy window of 1.946 keV centered at 511 keV to the count total in the annihilation peak. The W parameter was calculated as the fraction of counts in the energy interval 515.66 – 519.72 keV and 502.67 – 506.74 keV.

3. Results

3.1. Positron lifetime measurements

The evolution of τ_1 , τ_2 , $\langle \tau \rangle$ and I_2 as a function of annealing temperature is represented in Figures 1 and 2. All the alloys exhibited a two-component spectrum through the annealing temperature range except Fe14CrY in the as-HIP condition, which yielded a single-component after annealing at $950^\circ\text{C} < T < 1350^\circ\text{C}$, see Figure 1a). The lifetime

value of the second component, τ_2 , for Fe14Cr heat treated after forging decays monotonously from ~480 ps to ~360 ps through the temperature range, see Figure 2c). In contrast, the ODS alloys presented a visible recovery of the τ_2 value with onset at temperatures between 750 and 950 °C, which seems to depend on the treatments underwent after their HIP consolidation as the plots represented in Figures 1 and 2 reveal. Up to the recovery temperature, the τ_2 value remained essentially constant for these alloys except for Fe14CrY in the as-forged condition. After annealing at $T < 950$ °C the mean value of τ_2 resulted in (350 ± 40) ps and (293 ± 24) ps for Fe14CrY in the starting conditions as-HIP and heat treated after forging, respectively, (269 ± 9) ps for Fe14CrYWTi heat treated after forging and (291 ± 12) ps for heat treated Fe14CrWTiY. In order to emphasize the changes accompanying the recovery, the dispersion in the I_2 values was limited constraining τ_2 to the mean value above quoted for the corresponding spectra. Short lifetime values, ranging between 110 and ~200 ps in these alloys, may be attributed to positron annihilation at an abundant variety of defects inherent to their complex microstructure such as single vacancies, divacancies or trivacancies, impurity-vacancy complex, dislocations or defects associated with them as jogs, vacancies and impurity-vacancy complexes, defects at grain boundaries and interfaces, as well as defects related with second-phase precipitates [14, 25, 26]. Positron lifetime values between 220 and 400 ps appear to be characteristic of annihilation in tridimensional vacancy clusters or nanovoids in α -Fe [27-29].

In the interpretation of the lifetime results the following remarks have to be considered. 1) The fact that positron lifetime spectra are inconsistent with a standard trapping model derives from the complex microstructure of these alloys as revealed by TEM analyses [22, 23, 30]. The high number density and variety of complex defects, heterogeneously distributed in many cases, prevent any precise and reliable information

about the defects contributing to the short lifetime component even though a diffusion-limited trapping model is applied. 2) Attempts for decomposing the short lifetime component in those spectra that exhibited a τ_1 value as high as ~ 200 ps, increasing the total number count of the spectra or constraining the lifetime values, failed. These analyses resulted in unrealistic lifetime values, or alternatively, either negative or meaningless intensity values with very large errors, and unacceptable variances. The above remarks point out that the second lifetime component that appears in the ODS alloys after annealing at 950°C would be essentially attributable to real changes in the positron traps induced by annealing. Moreover, specific information about the positron traps responsible for the short lifetime component cannot be achieved from the present results. Nevertheless, the partial recovery or transformation of these traps can be inferred from the changes in the lifetime τ_1 and intensity $I_1 = 1 - I_2$.

3.1a. Fe14CrY

Figure 1 summarizes the effect of the thermo-mechanical treatment on the annihilation parameters for the ODS Fe14CrY alloy. The second lifetime of 350 ps, present in the as-HIP condition, disappears completely after annealing at temperatures in the interval $950^\circ\text{C} < T < 1350^\circ\text{C}$ but a very strong second lifetime component of ~ 250 ps develops after annealing at 1350°C . This is observed along with a considerable reduction of the τ_1 value, which indicates thermal activated vacancy release from defects contributing to the short lifetime component and formation of new open-volume defects. The evolution of I_2 indicates the recovery onset of vacancy-type defects at 750°C , which means that the defects responsible for the 350 ps component become unstable and start to release vacancies. These migrating vacancies appear to flow to strong vacancy sinks contributing to the short lifetime component, as its lifetime value rises from (195 ± 2) ps

to (220 ± 1) ps up to developing tridimensional vacancy clusters that give rise to the observed second lifetime component of ~ 250 ps.

The alloy in the as-forged condition exhibits an initial second lifetime component of 260 ps with a much higher intensity I_2 than the one for the alloy in the as-HIP condition, 28% against 1.2%, see the corresponding plots in Figure 1. After annealing at 150 °C, I_2 goes down to 9% and τ_2 increases to ~ 400 ps. These values remain practically constant after the successive anneals up to 750 °C. This indicates that a significant part of the defects responsible for this 260 ps component being smaller in size and very much abundant than those of 350 ps in the as-HIP samples are unstable at 150 °C. It should be noted that the forged material in the air-cooled condition may retain vacancies frozen as complex vacancy clusters. The vacancy release from these defects at 150 °C appears to promote coarsening of other more stable defects, although in competition with other vacancy sinks. The latter may be some of the defects that contribute to the short lifetime as the simultaneous increment in τ_1 and I_1 shows. At $T > 750$ °C the τ_2 and τ_1 values start to recover simultaneously. This can be interpreted as dissolution of the large voids responsible for the ~ 380 ps component and trapping of the released vacancies in some of the defects contributing to short positron lifetime, which turn into tridimensional vacancy clusters, or nanovoids. These clusters with lifetime values of (242 ± 7) ps survive after annealing at 1400 °C, for 90 minutes at least. This interpretation would be compatible with the fact that the $\langle \tau \rangle$ value is unaltered after the recovery of the 380 ps traps, see Figure 1b). As an alternative interpretation one can conceive that defects responsible for the lifetime of ~ 240 developed after annealing at $T > 750$ °C were actually present before but contributing to the short lifetime component. Then, it would be resolved by the fits after annealing out the 380 ps defects. However, if

the number density of the 240 ps defects is unchanged after annealing at $T > 750\text{ }^{\circ}\text{C}$ the $\langle \tau \rangle$ value should very likely decrease instead of remaining essentially constant.

The unexpected large uncertainty in the I_2 value for the as-forged samples after the isochronal anneal at $850\text{ }^{\circ}\text{C}$, confirmed repeating the measurements at least 3 times, demanded attention, see Figure 1b). Thus, isothermal annealing experiments at $800\text{ }^{\circ}\text{C}$ and $850\text{ }^{\circ}\text{C}$ were performed on a pair of samples starting from the as-forged and air-cooled condition. The results are summarized in Table 1. After isothermal annealing for 30 min at $800\text{ }^{\circ}\text{C}$ the second lifetime component yields I_2 and τ_2 values of $(13 \pm 17)\%$ and (265 ± 50) ps, which remain essentially constant after isothermal annealing for 270 min. The subsequent isothermal annealing at $850\text{ }^{\circ}\text{C}$ for 30 min induces a remarkable increase in the I_2 value and in its uncertainty, as well as a reduction in τ_2 . Afterwards, the I_2 and τ_2 values appear to be constant after annealing beyond 90 min. It is worth noticing that the τ_1 value remains constant after isothermal annealing at $800\text{ }^{\circ}\text{C}$ longer than 30 min, but it lowers remarkably after isothermal annealing at $850\text{ }^{\circ}\text{C}$ and becomes again constant when the annealing time is above 90 min. This appears to reproduce the τ_1 behavior at the recovery onset of τ_2 in the as-forged Fe14CrY samples isochronally annealed, as the corresponding plot in Figure 1b) and results in Table 1 show.

The evolution of I_2 for the Fe14CrY samples heat treated after forging exhibits an isochronal annealing behavior very similar to that for the samples in as-HIP condition, except for the vanishing of second lifetime component, as the comparison between the plots in Figure 1 reveals. After annealing at $1050\text{ }^{\circ}\text{C}$, I_2 rises from 10 to 92 % accompanied by a drop in τ_2 from 293 ± 24 to 218 ± 3 ps. At temperatures above $1050\text{ }^{\circ}\text{C}$, I_2 decreases and τ_2 increases, ending at values of $\sim 60\%$ and ~ 245 ps after the final anneal at $1400\text{ }^{\circ}\text{C}$, in concordance with the corresponding values for the other two pairs of Fe14CrY samples. In the samples heat treated after forging it is worth noticing the

clear correlation of the onset of the I_2 recovery at 750 °C with the rise of τ_1 , as well as the simultaneous correspondence between the maximum values of I_2 with the minimum τ_1 values, as the plots in Figure 1c) show. This correspondence is also evident in the other two pair of samples although it occurs at different temperatures.

Regarding the evolution of the mean positron lifetime $\langle \tau \rangle$ with isochronal annealing no significant changes are observed for the samples in the as-HIP or as-forged conditions. For the samples heat treated after forging, $\langle \tau \rangle$ appears to slightly rise after annealing at 950 °C remaining constant until 1350 °C, and then decreases just below the initial value.

3.1b. *Fe14CrYWTi and Fe14CrWTiY*

As stated in Section 2, the starting conditions for the samples of these two alloys were different: thermal treatment at 850 °C after forging for Fe14CrYWTi and heat treatment at 1300 °C for Fe14CrWTiY. Nevertheless, either alloys exhibit decrease of the I_2 above 750 °C accompanied by a rise of τ_1 in the same way as the Fe14CrY alloy, see the plots in Figure 2. Afterwards, τ_1 and τ_2 recover in coincidence with a steeply increase in I_2 up to attaining a maximum value after annealing at ~1150 °C. Beyond this temperature, τ_1 and τ_2 are practically constant and the mean lifetime $\langle \tau \rangle$ drops due to the decrease of the intensity I_2 , which implies annealing out of the open volume defects responsible for the second lifetime component being more evident for Fe14CrYWTi.

3.1c. *Fe14Cr*

The recovery characteristics of this non-ODS alloy, heat treated at 850 °C after forging, differ noticeably from those observed for the ODS alloys. The lifetime τ_2 does not exhibit the distinctive steep recovery of the ODS alloys at 800 – 1000 °C but a

gradual reduction starting after annealing above 250 °C as the plots in Figures 1 and 2 reveal. Moreover, the recovery of $\langle \tau \rangle$ occurs at 1050 °C corresponding with the continuous I_2 decrease and a constant τ_1 value. Preceding this recovery, I_2 increases at the same time that the reduction in the τ_1 value occurs for annealing above 750 °C. This is also interpreted as evidence of vacancy release from defects contributing to the first lifetime component and subsequent formation of new voids like it occurs for the ODS alloys. In addition, it appears that Fe14Cr heat treated after forging exhibits an initial I_2 decreases concurrently with a considerable increase of the τ_2 value after annealing at 150 °C. This can be the result of vacancy release from unstable vacancy clusters and their competitive trapping in defects responsible for the first lifetime component, and in stable voids that grow.

3.2. CDB measurements

The characteristics of the ratio CDB curves and their evolution with isochronal annealing are shown for selected annealing temperatures in Figures 3 and 4, along with the ratio curves for the reference samples of the alloying elements and Y_2O_3 . All the CDB curves at a given annealing temperature are normalized to the one for Fe14Cr annealed at the corresponding temperature. No significant changes respect to the Fe14Cr samples are found in the low-momentum region, i.e. for $p_L < 10 \times 10^{-3} m_0 c$, after annealing at temperatures $T < 950$ °C. In this region some changes are evident after annealing at $T \geq 950$ °C, except for the Fe14CrYWTi samples. By contrast, the annealing effect on the high-momentum side of the ratio curves of the ODS alloys is obvious. The remarkable reduction of the positron annihilations with high-momentum electrons, relative to the Fe14Cr alloy, appears to be related to a major contribution of the core electrons of Cr, or other alloying elements such as Y, W, Ti and Si, in the annihilation

events. Nevertheless, the effective changes over the high-momentum side appear not to follow a defined pattern revealing the characteristic signature of a particular alloying element. This result can be interpreted as evidence for competitive positron trapping in defects with a configurational surrounding that can either concurrently or separately contain Cr, Y and other alloying impurities.

Figure 5 shows the W - S correlation plots for all the samples. These plots are useful for revealing the presence of different positron traps or changes in the chemical surrounding of the positron annihilation sites during isochronal annealing. It is known in the case of positron annihilation taking place in two positron states, i.e. in a free state and in a trapped state in a single type of defect, or otherwise in two trapped state in two different types of defect, the measured line shape parameters S and W are given by [31]

$$\begin{aligned} S &= f_1 S_1 + (1 - f_1) S_2 \\ W &= f_1 W_1 + (1 - f_1) W_2 \end{aligned} \quad (2)$$

where S_i stand for the line shape parameters representative of the annihilations with the low momentum valence electrons for each state, and W_i the corresponding with the high momentum electrons. From Equation 2 the following correlation is found

$$W = -RS + (W_2 + RS_2) \quad (3)$$

where R is a constant defect specific parameter independent of the number density of positron traps given by

$$R = \frac{W_1 - W_2}{S_2 - S_1} = \frac{W - W_2}{S_2 - S} \quad (4)$$

and the measured values of S and W are in the range $S_1 < S < S_2$ and $W_2 < W < W_1$.

Then, if the W - S plot exhibits a full linear dependence, either a single type of defect acts

as positron traps or there exists positron trapping saturation in two effective defects through the recovery and isochronal annealing. This is the case for non-ODS Fe14Cr, see the corresponding plot in Figure 5. In contrast, the plots for the ODS alloys only exhibit a linear dependence after annealing at $T > 1150\text{ }^{\circ}\text{C}$ except for Fe14CrWTiY heat treated at $1300\text{ }^{\circ}\text{C}$.

4. Discussion

4.1. Fe14CrY

4.1a. As-forged samples

Among the different samples investigated, it is expected that the ODS Fe14Cr samples in the as-forged condition achieve the most far out of equilibrium microstructure because of the fast cooling rate after forging at $1100\text{ }^{\circ}\text{C}$. The large increase of τ_2 simultaneously with the significant drop of I_2 after annealing at $150\text{ }^{\circ}\text{C}$ reveals thermal shrinking of metastable vacancy clusters and coarsening of stable ones via trapping of migrating vacancies. These large tridimensional clusters or voids are thermally stable up to $750\text{ }^{\circ}\text{C}$. Above this temperature these voids become unstable, the representative positron lifetime τ_2 for the voids drops steeply and the intensity I_2 rises simultaneously, see Figure 1b). This can only be interpreted as a sign of development of new vacancy clusters at the expenses of the vacancies released from unstable voids during their thermal shrinkage. The characteristic τ_2 value for the new clusters results to be 235 ± 10 ps after annealing at $T \geq 950\text{ }^{\circ}\text{C}$. The fact that the W - S plot for these samples exhibits a constant R value of 0.2330 ± 0.0010 for annealing temperatures $T > 1150\text{ }^{\circ}\text{C}$ concurrent with the constant value of τ_2 supports the above interpretation. These clusters, as well as those appearing in the temperature range $150 - 750\text{ }^{\circ}\text{C}$, must be associated with some

1
2
3 solute impurities that stabilize them in the corresponding temperature range. According
4
5 with the calculi of the positron lifetime for tridimensional vacancy clusters in pure α -Fe,
6
7 these clusters could contain a number of 3 to 5 vacancies if solute impurities are not
8
9 found associated with them [25, 26], but they would be unstable at 150 °C [22]. Some
10
11 impurities would therefore have to be associated with the stable vacancy clusters.
12
13 Hence, the binding of solute atoms to these clusters would be reflected on the high-
14
15 momentum region of the CDB spectrum by the contribution of core electrons from the
16
17 solute atoms. After any annealing step, the high-momentum region of the CDB curves
18
19 for Fe14CrY in the as-forged condition seems to exhibit characteristics compatible with
20
21 both the Cr and Y signature, see Figure 3. No conclusive evidence for the association of
22
23 vacancy clusters with an exclusive atom, i.e. either Cr or Y atoms, can be attained from
24
25 these curves. Thus, the changes in the high-momentum region induced by successive
26
27 isochronal annealing can be interpreted as the result of the concurrent contribution of
28
29 core electrons from Cr and Y atoms associated with the positron traps.
30
31
32
33
34
35
36
37

38 *4.1b. Heat-treated samples after forging*

39
40 The effect of the heat treatment at 850 °C after forging is to shift the edge of the abrupt
41
42 changes in I_2 , τ_2 and τ_1 from 750 °C to 950 °C, see Fig 1c). Nevertheless, these changes
43
44 are preceded by a recovery of I_2 and a rise of τ_1 indicating that: 1) some unstable
45
46 vacancy clusters still remain after the pre-treatment at 850 °C for 2 h, and 2) there exists
47
48 a flow of the vacancies released from the shrinking clusters to some defects that
49
50 contributes to the first lifetime component, as occurs for the samples annealed in the as-
51
52 forged condition. These defects would have capability for trapping vacancies giving rise
53
54 to a variety of positron traps apparently stable at 1050 °C. Above this temperature, I_2
55
56 decreases rapidly with a simultaneous increase of τ_2 , which suggests shrinkage of some
57
58
59
60

clusters and coarsening of others. However, the last anneal at 1400 °C lowers considerably the τ_2 , τ_1 and $\langle \tau \rangle$ values revealing unstability of the defects, see Figure 1c). In these samples the linear correlation between the parameters W and S is also apparent after annealing at $T > 1150$ °C with a parameter R of 0.2590 ± 0.0021 as the corresponding plot in Figure 5 reveals. For annealing at $T \leq 1150$ °C the W and S values are found apparently randomly distributed in a bound region suggesting a complex annihilation scheme in the samples with positron annihilations in more than two states. In contrast, this concentration of the W and S values does not occur for the as-forged samples. This difference in the evolution of the parameters W and S can be attributed to the pre-treatment at 850 °C.

The comparison of the ratio CDB spectra with those for the as-forged samples reveals that the fast recovery of I_2 after annealing at $T > 1150$ °C is related to a considerable reduction of the Cr and Y contribution to high-momentum annihilations, see Figure 3. The above and the fact that the defects induced by annealing at 1050 °C are clearly unstable at higher temperatures in the heat treated samples, in parallel with the significant drop of $\langle \tau \rangle$ after annealing at 1400 °C, would indicate a relationship between the thermal stability of the defects and the presence of Y and Cr atoms in their surroundings.

4.1c. As-HIP samples

These samples through isochronal annealing at $T \leq 950$ °C replicate the evolution of the positron lifetime parameters observed in the samples heat treated after forging, see Figure 1. Now, I_2 for $T \leq 950$ °C is considerably smaller, and τ_2 and τ_1 larger, than the corresponding values for the samples heat treated after forging. However, it is worth to notice that in any case the $\langle \tau \rangle$ values for the Fe14CrY alloy coincide just at the starting

of the isochronal annealing experiments irrespective of the previous thermo-mechanical treatment. This result reveals that the HIP consolidated ODS Fe14Cr alloy contains an effective concentration of positron traps high enough to attain trapping saturation despite the subsequent treatments herein applied.

At temperatures above 950 °C, the vacancy clusters responsible for the lifetime component of 350 ps anneal out, and a single lifetime component emerges gradually increasing its lifetime up to a value of 220 ± 1 ps upon annealing at 1250 °C. It is worth to be aware that the lifetime of the vacancy clusters growing after annealing at 1050 °C is 218 ± 3 ps in the samples heat-treated after forging and 221 ± 3 in the as-forged samples. Then, the single lifetime component of 220 ps appears to be due to positron annihilation saturation in the vacancy clusters grown by annealing, which coarsen at $T > 1250$ °C while their concentration declines as the plot in Figure 1a) reflects. This interpretation is supported by the corresponding W - S plots in Figure 5. Now, in opposition to that occurring for the other two Fe14CrY samples the lineal W dependence on S for $T > 1150$ °C is decreasing with annealing temperature resulting in a defect specific parameter R of 0.349 ± 0.019 . Furthermore, the random evolution of the data points through isochronal annealing at $T \leq 1150$ °C reflects a starting defect structure in these samples that differs from those in the other two pair samples thermo-mechanically treated.

4.2. Fe14CrYWTi heat-treated samples after forging

The evolution of the lifetime parameters with isochronal annealing for these samples exhibits significant coincidences with the ODS Fe14Cr samples submitted to the same thermo-mechanical treatment as the respective plots in Figures 1c) and 2a) reveal. These are: 1) the I_2 recovery onset above 750 °C and simultaneous increase of τ_1 , and 2) the

development of new vacancy clusters at $T > 950$ °C revealed by the abrupt rise of I_2 concurrently with a considerable drop in τ_1 and τ_2 . By contrast, there exist evident differences: 1) at $T > 1150$ °C, a remarkable recovery of the mean positron lifetime $\langle \tau \rangle$ appears with its onset at 1150 °C while the τ_1 and τ_2 values remain practically constant; and 2) at $T < 1050$ °C, the second lifetime component due to vacancy clusters yield I_2 values at least ~ 2.5 times higher than those for the Fe14CrY samples, and τ_2 values considerably smaller, i.e. 270 ps against 292 ps. These noteworthy differences respect to the counterpart Fe14CrY samples can only be attributed to the W and Ti addition. Nevertheless, a linear relationship between W and S like the one for the Fe14CrY samples is satisfied after annealing at $T > 1150$ °C with a parameter $R = 0.322 \pm 0.006$, see the plots in Figure 5. For annealing a $T \leq 1150$ °C the parameters W and S are found bounded inside an interval of values even narrower than the one for the counterpart pair of Fe14CrY samples being also attributable to the effect of the heat treatment at 850 °C after forging. As the I_2 value scales with the number concentration of the vacancy-type defects responsible for this lifetime component, and τ_2 does it with the size, the positron lifetime results indicate that either W or Ti promotes the formation and refinement of the vacancy clusters. Since TEM studies of ODS Fe14CrWTi have revealed the capability of Ti for improving the dispersion of oxide particle via its incorporation into the oxide particle [32], the aforementioned differences should accordingly be associated with the Ti effect on the dispersion.

4.3. Fe14CrWTiY heat-treated at 1300 °C

The changes in the lifetime parameters for these samples are qualitatively similar to those found in Fe14CrYWTi as the plots in Figure 2 show, even though the respective pre-treatments were very different. A small recovery stage of I_2 at $T > 750$ °C followed

by a strong rise of I_2 , and a second recovery at $T > 1150^\circ\text{C}$ appear, which are accompanied by qualitative changes in τ_2 , τ_1 and $\langle \tau \rangle$ similar to those observed in the Fe14CrYWTi samples. The fact that the I_2 values after annealing at $T \leq 750^\circ\text{C}$ are a factor of ~ 1.5 to 2 smaller than the ones for Fe14CrYWTi may be attributed to annealing induced by the pre-treatment at 1300°C for 1 h. But, it should be noted that after the final isochronal anneals at 1350°C and 1400°C , which were longer in time than the pre-treatment for Fe14CrYWTi, I_2 and $\langle \tau \rangle$ for Fe14CrWTiY stay at values significantly higher than those for Fe14CrYWTi, i.e. 50 % and 200 ps against 40 % and 170 ps. This result is compatible with a possible presence of defects more stable than the ones present in Fe14CrYTiW. This possibility is supported by the TEM analyses accomplished in these samples that evidence a clear effect of the unintentional Si impurities on the oxide dispersion characteristics developed [21]. It was found that complex Y-Si oxide nanoparticles developed predominantly instead of Y-Ti oxide dispersoids. In that case, the high stability of vacancy clusters in these samples might be attributed to their association with the Y-Si oxide dispersoids or Si solutes.

The W - S plot for Fe14CrWTiY exhibits a clear difference respect to those for the other ODS alloys, see Figure 5. The transition to a linear correlation between W and S after annealing at $T > 1150^\circ\text{C}$ is no longer evident, being very likely attributable to the pre-treatment at 1300°C . As a result the W and S values appear not to be correlated with the annealing temperature over the whole temperature range. This means that the nano-features resulting in these samples is more complex than those for the other ODS alloys, which could be attributed to the effect of Si impurities present in these samples according with the above discussion. As occurs in the Fe14CrY alloy, the ratio CDB spectra shown in Figure 4 do not exhibit any clear sign attributable to any of the alloying impurities over the whole range of annealing temperature. The ratio CDB

curves for reference samples of Si is also represented in Figure 4 to assess the Si effect on the enhanced stability of the vacancy clusters in the Fe14CrWTiY alloy unintentionally contaminated with Si. Moreover, the shape and evolution of the high-momentum side of the spectra being quite similar to the ones for Fe14CrY suggest a minor participation of the core electrons from W, Ti and Si in the positron annihilations. At present, a consistent explanation of the enhanced stability of the vacancy defects developed in the Fe14CrWTiY samples cannot be given except that it is likely due to the thermo-mechanical treatments underwent by the samples.

5. Conclusions

Positron annihilation measurements were performed on samples of the ODS Fe14Cr and Fe14CrWTi alloys submitted to sequential isochronal annealing. The main findings are summarized as follows:

- (1) Irrespective of the starting conditions of the samples, the results revealed the presence of tridimensional vacancy clusters, or defect nano-features, some of which can survive annealing at 1400 °C for 90 min, at least.
- (2) The evolution of the positron annihilation characteristics shows two recovery stages for these vacancy type defects. The first one starting at $T > 750$ °C is attributed to thermal shrinkage of large vacancy clusters, or voids, and consequent trapping of the released vacancies by other defects of different nature.
- (3) Annealing in the temperature interval $800 < T \leq 1050$ °C gives rise to new vacancy clusters, whose number concentration is considerably higher than the one for the vacancy clusters existing at $T \leq 750$ °C. The new vacancy clusters start to anneal out at $T > 1050$ °C in the Fe14CrY samples and at $T > 1150$ °C in Fe14CrYWTi

and Fe14CrWTiY. In the case of the Fe14CrY samples isochronally annealed starting from the as-forged condition, the new clusters appear to exhibit the highest thermal stability.

- (4) The number concentration of the vacancy clusters present in the Fe14CrYWTi samples after annealing at $T \leq 750$ °C is considerable higher, and their size smaller, compared with the corresponding ones in the Fe14CrWTiY samples. However, the major part of vacancy defects developed upon annealing at ~950 °C result to be remarkably more stable in Fe14CrWTiY than in Fe14CrYWTi.
- (5) The W-S plots for the ODS Fe14Cr and Fe14CrYWTi alloys reveal a clear transition in the relationship between these parameters after annealing at temperatures above 1050 °C. This is compatible with a change in the structure of the nano-features present in these alloys. This transition is not present in non-ODS Fe14Cr alloys or in the case of the ODS Fe14CrWTiY alloy pre-heated at 1300 °C.

Acknowledgments

This investigation was supported by the Spanish Ministry of Economy and Competitiveness (project ENE2012-39787-C06-05), Comunidad de Madrid (Spain) through the MULTIMATCHALLENGE (S2013/MIT-2862) and TECHNOFUSION (II)-CM (S2013/MAE-2745) programs, and European Commission through the European Fusion Development Agreement (contracts 09-240 and 10-425).

References

- [1] S. Ukai, and M. Fujiwara, J Nucl Mater, 307 (2002) 749-757.
- [2] L.K. Mansur, A.F. Rowcliffe, R.K. Nanstad, S.J. Zinkle, W.R. Corwin, and R.E. Stoller, J Nucl Mater, 329 (2004) pp. 166-172.
- [3] K.L. Murty, and I. Charit, J Nucl Mater, 383 (2008) pp. 189-195.

- [4] G.R. Odette, M.J. Alinger, and B.D. Wirth, *Annu Rev Mater Res*, 38 (2008) pp. 471-503.
- [5] D.J. Larson, P.J. Maziasz, I.S. Kim, and K. Miyahara, *Scripta Mater*, 44 (2001) pp. 359-364.
- [6] V. de Castro, E.A. Marquis, S. Lozano-Perez, R. Pareja, and M.L. Jenkins, *Acta Mater*, 59 (2011) pp. 3927-3936.
- [7] M.K. Miller, and C.M. Parish, *Mater Sci Tech-Lond*, 27 (2011) pp. 729-734.
- [8] A. Hirata, T. Fujita, Y.R. Wen, J.H. Schneibel, C.T. Liu, and M.W. Chen, *Nat Mater*, 10 (2011) pp. 922-926.
- [9] C.A. Williams, P. Unifantowicz, N. Baluc, G.D.W. Smith, and E.A. Marquis, *Acta Mater*, 61 (2013) pp. 2219-2235.
- [10] C.A. Williams, G.D.W. Smith, and E.A. Marquis, *Scripta Mater*, 67 (2012) 108-111.
- [11] P. He, M. Klimenkov, R. Lindau, and A. Moslang, *J Nucl Mater*, 428 (2012) pp. 131-138.
- [12] T. Liu, H. Shen, C. Wang, and W. Chou, *Mater Res Innov*, 18 (2014) pp. 410-413.
- [13] Z.H. Yao, W.H. Xiong, G.P. Zhang, X. Chen, and B. Huang, *Mater Design*, 56 (2014) pp. 953-958.
- [14] Y. Ortega, V. de Castro, M.A. Monge, A. Munoz, T. Leguey, and R. Pareja, *J Nucl Mater*, 376 (2008) pp. 222-228.
- [15] J. Xu, C.T. Liu, M.K. Miller, and H.M. Chen, *Phys Rev B*, 79 (2009).
- [16] Y. Ortega, M.A. Monge, V. de Castro, A. Munoz, T. Leguey, and R. Pareja, *J Nucl Mater*, 386-88 (2009) pp. 462-465.
- [17] R. Pareja, P. Parente, A. Munoz, A. Radulescu, and V. de Castro, *Philos Mag*, 95 (2015) pp. 2450-2465.
- [18] R.W. Siegel, *Annu Rev Mater Sci*, 10 (1980) pp. 393-425.
- [19] M.J. Puska, and R.M. Nieminen, *Rev Mod Phys*, 66 (1994) pp. 841-897.
- [20] P. AsokaKumar, M. Alatalo, V.J. Ghosh, A.C. Kruseman, B. Nielsen, and K.G. Lynn, *Phys Rev Lett*, 77 (1996) pp. 2097-2100.
- [21] M.A. Auger, T. Leguey, A. Munoz, M.A. Monge, V. de Castro, P. Fernandez, G. Garces, and R. Pareja, *J Nucl Mater*, 417 (2011) pp. 213-216.
- [22] M.A. Auger, V. de Castro, T. Leguey, M.A. Monge, A. Munoz, and R. Pareja, *J Nucl Mater*, 442 (2013) S142-S147.

- [23] M.A. Auger, V. de Castro, T. Leguey, J. Tarcisio-Costa, M.A. Monge, A. Munoz, and R. Pareja, *J Nucl Mater*, 455 (2014) pp. 600-604.
- [24] P. Kirkegaard, N.J. Pedersen, and M. Eldrup, *Risø Report M2740*, Risø National Laboratory, Denmark, (1989).
- [25] A. Vehanen, P. Hautojarvi, J. Johansson, J. Ylikauppila, and P. Moser, *Phys Rev B*, 25 (1982) pp. 762-780.
- [26] V. Krsjak, Z. Szaraz, and P. Hahner, *J Nucl Mater*, 428 (2012) pp. 160-164.
- [27] M.J. Puska, and R.M. Nieminen, *J Phys F Met Phys*, 13 (1983) pp. 333-346.
- [28] H. Ohkubo, Z. Tang, Y. Nagai, M. Hasegawa, T. Tawara, and M. Kiritani, *Mat Sci Eng A-Struct*, 350 (2003) pp. 95-101.
- [29] J. Kuriplach, O. Melikhova, C. Domain, C.S. Becquart, D. Kulikov, L. Malerba, M. Hou, A. Almazouzi, C.A. Duque, and A.L. Morales, *Appl Surf Sci*, 252 (2006) pp. 3303-3308.
- [30] M.A. Auger, T. Leguey, V. de Castro, M.A. Monge, and R. Pareja, *Mater Sci Tech-Lond*, 30 (2014) pp. 1704-1708.
- [31] X. Wu, K.R. Hebert, P. Asoka-Kumar, and K.G. Lynn, *J. Electrochem. Soc.*, 141 (1994) pp. 3361-3368.
- [32] A. Hirata, T. Fujita, C.T. Liu, and M.W. Chen, *Acta Mater*, 60 (2012) pp. 5686-5696.

Table 1: Isothermal annealing effect on the positron lifetime spectrum of as-forged Fe14CrY.

Fe14CrY	Annealing time (min)	τ_1 (ps)	τ_2 (ps)	I_2 (%)	$\langle \tau \rangle$ (ps)
As-forged	---	180±7	256±16	29±12	202±60
+ Annealed at 800 °C	30	189±8	265±50	13±17	199±80
	90	188±7	273±40	13±12	199±60
	270	188±6	278±40	13±11	200±60
+ Annealed at 850 °C	30	154±50	217±22	70±50	204±200
	90	120±30	209±3	89±7	199±20
	270	119±13	217±3	80±4	197±18

Figure 1. Isochronal annealing effect on the positron lifetime parameters for the ODS Fe14Cr alloy (Fe14CrY) in different conditions: a) as-HIP, b) as-forged and c) heat treated after forging.

Figure 2. Isochronal annealing effect on the positron lifetime parameters for the alloys: a) Fe14CrYWTi heat treated at 850 °C after forging, b) Fe14CrWTiY heat treated at 1300 °C and c) non-ODS Fe14Cr heat treated at 850 °C after forging.

Figure 3. CDB ratio spectra for the ODS Fe14CrY alloy isochronally annealed at different temperatures. The starting conditions of the samples were (-●-) as-HIP, (-■-) as-forged and (-▲-) heat treated at 850 °C after forging. The CDB ratio curves for Fe, Cr and Y₂O₃ are shown for comparison.

Figure 4. Isochronal annealing effect on the CDB ratio spectra for (-●-) Fe14CrYWTi heat treated at 850 °C after forging, and (-■-) Fe14CrWTiY heat treated at 1300 °C. The CDB ratio curves for Fe, Cr, W, Ti, Si and Y₂O₃ oxide are shown for comparison.

Figure 5. S-W plots obtained from CDB data for the ODS and non-ODS Fe14Cr alloys isochronally annealed.

1
2
3
4
5
6
7
8
9
10
11
12
13
14
15
16
17
18
19
20
21
22
23
24
25
26
27
28
29
30
31
32
33
34
35
36
37
38
39
40
41
42
43
44
45
46
47
48
49
50
51
52
53
54
55
56
57
58
59
60

Table 1: Isothermal annealing effect on the positron lifetime spectrum of as-forged Fe14CrY.

Fe14CrY	Annealing time (min)	τ_1 (ps)	τ_2 (ps)	I_2 (%)	$\langle \tau \rangle$ (ps)
As-forged	---	180±7	256±16	29±12	202±60
+ Annealed at 800 °C	30	189±8	265±50	13±17	199±80
	90	188±7	273±40	13±12	199±60
	270	188±6	278±40	13±11	200±60
+ Annealed at 850 °C	30	154±50	217±22	70±50	204±200
	90	120±30	209±3	89±7	199±20
	270	119±13	217±3	80±4	197±18